Electronic structure and volume effect on thermoelectric transport in *p*-type Bi and Sb tellurides

Min Sik Park,[1] Jung-Hwan Song,[2,*] Julia E. Medvedeva,[1] Miyoung Kim,[3] In Gee Kim,[4] and Arthur J. Freeman[2]

[1]*Department of Physics, Missouri University of Science and Technology, Rolla, Missouri 65409, USA*
[2]*Department of Physics and Astronomy, Northwestern University, Evanston, Illinois 60208, USA*
[3]*Division of Energy System Research, Ajou University, Suwon 443-749, Republic of Korea*
[4]*Graduate Institute of Ferrous Technology, Pohang University of Science and Technology, Pohang 790-784, Republic of Korea*

Thermoelectric transport properties (Seebeck coefficient, S, and electrical conductivity, σ) of *p*-type Bi and Sb tellurides are investigated using a first-principles all-electron density-functional approach. We demonstrate that the carrier concentration, band gap, and lattice constants have an important influence on the temperature behavior of S and that the volume expansion by 5.5% in Sb_2Te_3 results in an increase in S by 33 $\mu V/K$ at 300 K. We argue that in addition to the electronic structure characteristics, the volume also affects the value of S and hence should be considered as an origin of the experimental observations that S can be enhanced by doping Sb_2Te_3 with Bi (which has a larger ionic size) in Sb sites or by the deposition of thick Bi_2Te_3 layers alternating with thinner Sb_2Te_3 layers in a superlattice, Bi_2Te_3/Sb_2Te_3. We show that the optimal carrier concentration for the best power factor of Bi_2Te_3 and Sb_2Te_3 is approximately 10^{19} cm^{-3}.

The development of highly efficient thermoelectric (TE) materials is important for refrigeration and energy generation and storage technologies. The efficiency of TE materials is represented by the figure of merit, $ZT = S^2\sigma T/(\kappa_e + \kappa_L)$, where S is the Seebeck coefficient, σ is the electrical conductivity, and κ_e and κ_L are the electronic and lattice thermal conductivities, respectively. Thus, a higher ZT can be obtained by decreasing the denominator (smaller κ_e and/or κ_L) or by increasing the numerator (larger S and/or σ).[1,2] Although the thermoelectric materials have been extensively studied for the last decade, there are only a few theoretical simulations of their transport properties.[3,4]

Bi_2Te_3 alloys with peak $ZT \sim 1.0$ are well-known conventional materials for thermoelectric applications near room temperature.[5] In the experiments for Bi_2Te_3 and Sb_2Te_3-based alloys, the doping of bismuth and antimony atoms in Sb_2Te_3 and Bi_2Te_3, respectively, influences the thermoelectric properties,[6–8] where it is generally known that the antisite defects are the origin of the current carriers.[9–11] In addition, recently, the highest ZT value of ~ 2.4 was reported at 300 K in *p*-type Bi_2Te_3/Sb_2Te_3 superlattices.[12] Even though the phonon-blocking/electron-transmitting mechanism in the superlattice was suggested,[12] to our knowledge, the influence of the thickness and volume of each layer for the electronic transport coefficients of S and σ is not well understood. In this work, we first investigate the temperature-dependent behavior of the thermoelectric property in bulk Bi_2Te_3, $(Bi_{0.5}Sb_{0.5})_2Te_3$, and Sb_2Te_3; discuss the role of carrier concentration, band gap, and electronic structure; and compare the results to experiments. Second, we suggest that the dopant size effect by Bi and Sb cation doping can be one of the origins to influence the thermoelectric property, even though both Bi and Sb have the same number of valence electrons, and it is demonstrated that S in Sb_2Te_3 increases due to the volume expansion associated with the doping of larger Bi atoms.

For the study, we considered the rhombohedral structure for Bi_2Te_3 and Sb_2Te_3, and the hexagonal supercell structure[13] for $(Bi_{0.5}Sb_{0.5})_2Te_3$ where each

Bi (Sb) atom has four and two nearest neighbors of Sb (Bi) and Bi (Sb), respectively, in the hexagonal plane. We used experimental lattice constants for Bi_2Te_3 ($a_{BT} = 4.386$ Å, $c_{BT} = 30.497$ Å) and Sb_2Te_3 ($a_{ST} = 4.264$ Å, $c_{ST} = 30.458$ Å),[14,15] and average lattice constants for $(Bi_{0.5}Sb_{0.5})_2Te_3$. The internal atomic positions in $(Bi_{0.5}Sb_{0.5})_2Te_3$, Bi_2Te_3, and Sb_2Te_3 were optimized via force and total-energy minimization.[16,17] Experimentally, the Sb-doped Bi_2Te_3 shows *p*-type character;[6–8] therefore, we discuss only *p*-type Bi and Sb tellurides for comparing with experimental results. The electronic structure was calculated using the highly precise all-electron full-potential linearized augmented plane-wave (FLAPW) method in the local-density approximation (LDA) with spin-orbit coupling (SOC) included by a second variational method.[16,17] Further, the screened-exchange LDA (sX-LDA) method is used for obtaining correct band gaps at zero temperature. The sX-LDA method is known to provide a better description of the excited states and band gaps; in particular, good agreement with the experimental band gap (0.162 eV) was obtained for Bi_2Te_3 (0.154 eV).[18] To determine the Seebeck coefficient and the electrical conductivity, we employed the distribution function given by Boltzmann's equation in the constant relaxation-time approximation.[19] For the calculation of the group velocity, which is included in the transport coefficients, we use full intraband optical matrix elements defined within the FLAPW method. The thermoelectric transport coefficients of S and σ can, therefore, be calculated as

$$\mathbf{L}_{\alpha,\beta}^{(\nu)} = e^2\tau \int \frac{d\varepsilon d\mathbf{k}}{8\pi^3}\left(-\frac{\partial f_0}{\partial \varepsilon}\right)(\varepsilon - \mu)^\nu \delta(\varepsilon - \varepsilon_\mathbf{k})\mathbf{v}_\mathbf{k}^\alpha \mathbf{v}_\mathbf{k}^\beta, \quad (1)$$

$$\boldsymbol{\sigma} = \mathbf{L}^{(0)}, \quad \mathbf{S} = -\frac{1}{eT}(\mathbf{L}^{(0)})^{-1}\mathbf{L}^{(1)}, \quad (2)$$

where τ, f_0, and $\mathbf{v}_\mathbf{k}$ denote the relaxation time, Fermi-Dirac distribution function, and group velocity, respectively; e denotes the electrical charge; μ the chemical potential; T the
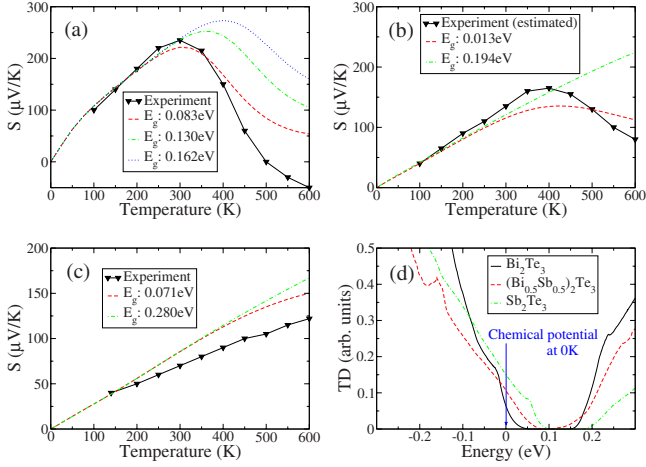
FIG. 1. (Color online) Temperature-dependent Seebeck coefficients of (a) Bi_2Te_3 at the carrier density of 1.32×10^{19} cm^{-3}, (b) $(Bi_{0.5}Sb_{0.5})_2Te_3$ at 3.16×10^{19} cm^{-3}, and (c) Sb_2Te_3 at 8.70×10^{19} cm^{-3}, where the experimental data are adapted from Ref. 6; and (d) the TDs defined by Eq. (1) for the cases with the band gap from the SOC-LDA.

temperature; and $\delta(\varepsilon - \varepsilon_{\mathbf{k}})$ the Dirac delta function. Different carrier concentration was treated within the rigid-band model[20] and a scissor operator[21] is applied to obtain the experimental band gaps in the transport coefficient calculations.

In previous experimental work, the thermoelectric properties of *p*-type $(Bi_{1-x}Sb_x)_2Te_3$ ($x=0.00$, 0.33, 0.39, 0.66, 0.71, and 1.00) were studied systematically.[6] Hence, for comparing with the experimental results, we have calculated S and σ for three *p*-type materials, Bi_2Te_3, $(Bi_{0.5}Sb_{0.5})_2Te_3$, and Sb_2Te_3, using a rigid-band shift that corresponds to the experimental carrier densities. Figure 1(a) shows three calculated Seebeck coefficients[22] of Bi_2Te_3 with the different band gaps at the experimental carrier density of 1.32×10^{19} cm^{-3} compared with experimental data. We here simulated the Seebeck coefficients with three different band gaps, i.e., 0.083 eV (SOC-LDA), 0.162 eV (extrapolated to 0 K from the measured values),[23] and 0.130 eV (measured at room temperature).[24] Below 300 K, all calculated results show excellent agreement with experiment, that is, a monotonic increase in S with temperature, which can be attributed to the very narrow energy window from the Fermi-Dirac statistics. Above 300 K, the overall Seebeck results show similar behavior to experiment; the different band gaps yield different S, and different peak temperatures at which a maximal peak of S appears, which is due to the compensated *p*-type contribution to Seebeck by thermally excited *n*-type carriers across the band gap. Thus, a larger band gap induces a higher peak temperature. The rapid decrease in $S(T)$ in the experiment compared to our results may be attributed to the band-gap reduction[24] and to dominant *n*-type defect creation at high temperatures.[10]

The 50% Sb-doped Bi_2Te_3 shows similar behavior to the Bi_2Te_3 case at low temperatures for the temperature dependent S in the experiment [Figs. 1(a) and 1(b)]. However, the peak shifts to a higher temperature (near 400 K) while the highest S value (170 μV/K) is lower—as compared to

Bi_2Te_3. In this case, the experimental carrier density of 3.16×10^{19} cm^{-3}, which is higher than that in Bi_2Te_3, is used. Since the experimental band gap is unknown for this composition, we used the sX-LDA method to obtain the correct band gap at zero temperature—0.194 eV, for $(Bi_{0.5}Sb_{0.5})_2Te_3$, which is between the experimental band gaps of 0.162 (Bi_2Te_3) and 0.280 eV (Sb_2Te_3).[23,25] We found that $S(T)$ with the sX-LDA band gap at low temperatures (below 400 K) is closer to the experimental one than that with the SOC-LDA band gap (0.013 eV). For Sb_2Te_3, the experimental carrier density of 8.70×10^{19} cm^{-3} is used. In Fig. 1(c), two calculated S's, in which the band gap of 0.071 eV (SOC-LDA) and 0.280 eV (experiment)[25] are used, are compared to the experimental value. Even though there is a difference between the S values of experiment and calculations, the trend in $S(T)$ up to 600 K is similar. The monotonically increasing behavior of S without the maximal peak comes from the large carrier density rather than the large band gap because the smaller band gap of 0.071 eV (SOC-LDA) also shows the increase in S instead of showing a peak near room temperature, as in Bi_2Te_3. This is also why the band gap has little effect on S in this simulation and yields very similar results for S between the two different band gaps, 0.071 and 0.280 eV.

To analyze the behavior of $S(T)$, we have calculated the transport distribution (TD),[3,4] which includes all necessary information, such as the group velocities and density of states,

$$TD_{\alpha,\beta}(\varepsilon) = \int d\mathbf{k} v_{\mathbf{k}}^\alpha v_{\mathbf{k}}^\beta \delta(\varepsilon - \varepsilon_{\mathbf{k}}). \qquad (3)$$

Here, the larger asymmetric TD below and above the chemical potential (i.e., a larger slope at the chemical potential) yields larger S. In Fig. 1(d), the transport distributions in three materials are plotted with respect to $\mu(0)$ and the chemical potential at 0 K. In Sb_2Te_3, the position of $\mu(0)$ is the furthest away from the valence-band maximum (VBM) compared to Bi_2Te_3 and $(Bi_{0.5}Sb_{0.5})_2Te_3$ because of its highest carrier density. This deep chemical potential in Sb_2Te_3 causes the highest peak temperature of S compared to $(Bi_{0.5}Sb_{0.5})_2Te_3$ and Bi_2Te_3. In addition, the largest TD, highest conductivity, yields the smallest $S(T)$ in Sb_2Te_3. Also, the overall steepest slope near the VBM of Bi_2Te_3 suggests that larger S in Bi_2Te_3 compared to $(Bi_{0.5}Sb_{0.5})_2Te_3$ and Sb_2Te_3 is partially due to the electronic structure differences as discussed below.

Figure 2(a) shows a comparison of the calculated S with experiment for all materials considered for various concentrations at 300 K. The theoretical results are in good agreement with experiment. The decrease in S as the carrier concentration increases, follows the general behavior of S in semiconductors. The carrier dependence of σ in Fig. 2(b) also shows usual behavior, that is, an increase in σ as the carrier concentration increases. Here, the constant relaxation-time (τ) value of 1.0×10^{-14} s is used. From the comparison between the theoretical and the experimental values, we can then fit τ's at 300 K to obtain 0.59×10^{-14}, 0.81×10^{-14}, and 2.16×10^{-14} s for Bi_2Te_3, $(Bi_{0.5}Sb_{0.5})_2Te_3$, and Sb_2Te_3, re-
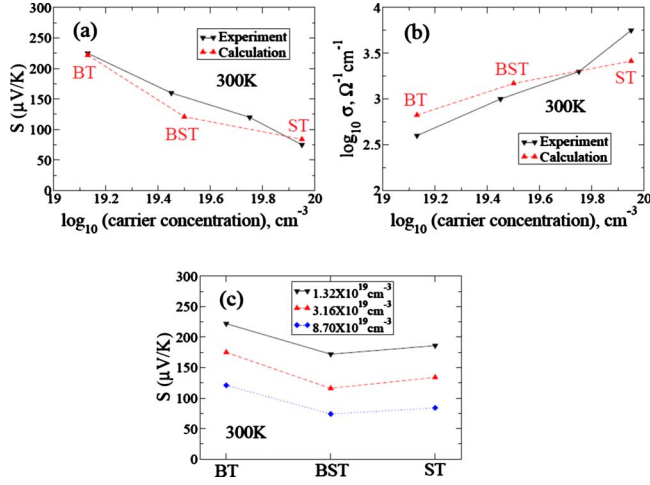
FIG. 2. (Color online) Carrier concentration dependent (a) Seebeck coefficients and (b) conductivities from the calculations for Bi_2Te_3 (BT), $(Bi_{0.5}Sb_{0.5})_2Te_3$ (BST), and Sb_2Te_3 (ST), and the experiment (adapted from Ref. 6); and (c) compound dependent Seebeck coefficients for each with the same carrier concentration.

FIG. 3. Band structures of the hexagonal (a) Bi_2Te_3, (b) $(Bi_{0.5}Sb_{0.5})_2Te_3$, and (c) Sb_2Te_3 in the SOC-LDA.

spectively, all of which have the same typical order of the previously assumed value, 10^{-14} s.[4] These fitted values also indicate a possible dramatic increase in the electronic contribution to the thermal conductivity when the Sb doping concentration becomes larger in Bi_2Te_3. Experimentally, the thermal conductivity of Bi_2Te_3 at 300 K does not change much, up to 75% Sb doping $(1.5–2 \text{ W m}^{-1} \text{ K}^{-1})$.[6] On the contrary, Bi_2Te_3 with Sb doping larger than 75% shows a large increase in $\kappa(2–4.5 \text{ W m}^{-1} \text{ K}^{-1})$. Hence, the relaxation-time values fitted for three different compositions above appear to have a correlation with the sharp increase in κ in the experiments. Due to this composition dependence of the relaxation time, we expect that the main contribution to the change in ZT for the variation in Sb doping concentration $<75\%$ is the power factor defined by $S^2\sigma$. To see the electronic structure effect for S, the S's are plotted at the same carrier concentrations for each compound in Fig. 2(c). The S's curves of $(Bi_{0.5}Sb_{0.5})_2Te_3$ and Sb_2Te_3 are similar and lower than Bi_2Te_3 that originates from the different contribution of electronic structure between Bi_2Te_3 and $(Bi_{0.5}Sb_{0.5})_2Te_3$, Sb_2Te_3, i.e., the different slopes between their TD's as seen in Fig. 1(d). However, it is difficult to explain the S behavior by the simple comparison between the band structures along high-symmetry lines such as counting the peaks near the VBM in Fig. 3. In fact, the band edges of these materials have been studied thoroughly and their VBMs are not located along the high-symmetry lines.[26,27]

As one of the possible origins for the change in the thermoelectric transport property by substitutional doping, the volume effect is investigated. Since the volume may change between Bi_2Te_3 (the higher limit) and Sb_2Te_3 (the lower limit) by the doping, we calculated the S's shown in Figs. 4(a) and 4(b) with three different lattice constants, namely, (a_{BT}, c_{BT}), $[a_{ave}=(a_{BT}+a_{ST})/2, \ c_{ave}=(c_{BT}+c_{ST})/2]$, and (a_{ST}, c_{ST}). The carrier concentration was kept constant and equal to 1.32×10^{19} cm^{-3} for comparison of the different lattice parameters and the experimental band gaps were used for Bi_2Te_3 and Sb_2Te_3.
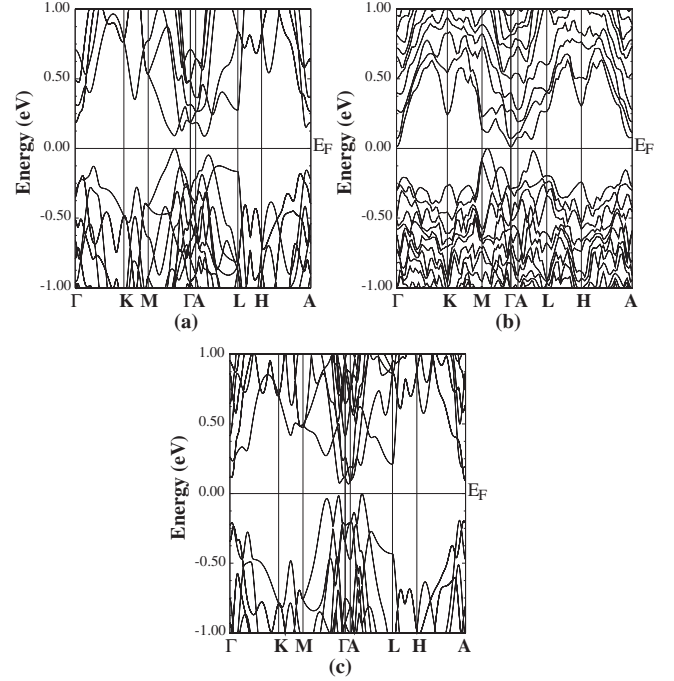
In Sb_2Te_3, with the increase in volume by 5.5% (from V_{ST} to V_{BT}), S increases by about 33 μV/K at 300 K, and the peak temperature with the highest S decreases from 575 to
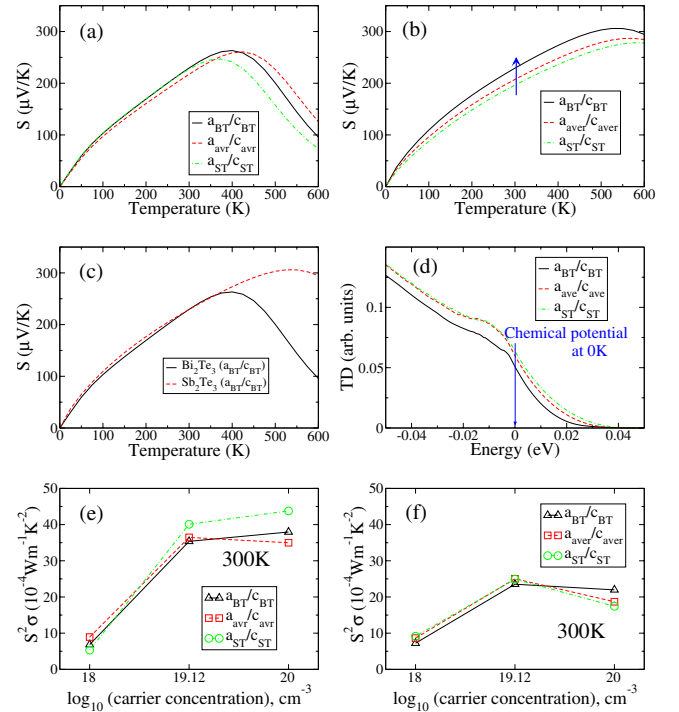

FIG. 4. (Color online) Temperature-dependent Seebeck coefficients at the carrier density of 1.32×10^{19} cm^{-3} of (a) Bi_2Te_3 and (b) Sb_2Te_3 with lattice constants a_{BT}/c_{BT}, a_{ave}/c_{ave}, and a_{ST}/c_{ST}; and of (c) Bi_2Te_3 and Sb_2Te_3 with the same lattice constant of a_{BT}/c_{BT}; and (d) TD's for the cases in Fig. 4(b); and carrier concentration dependent power factors at each lattice constant of (e) Bi_2Te_3 and (f) Sb_2Te_3.

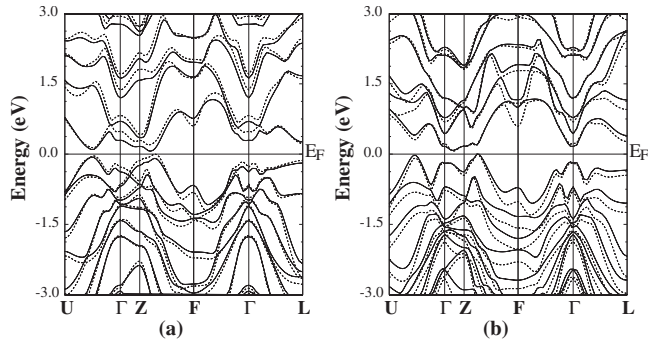FIG. 5. Band structures of the rhombohedral (a) Bi_2Te_3 and (b) Sb_2Te_3 with lattice constants a_{BT}/c_{BT} (solid line) and a_{ST}/c_{ST} (dotted line) in the SOC-LDA.

525 K in Fig. 4(b). One can expect that the volume increase causes "a larger number of carriers per unit cell" and thus a deeper chemical potential. Then if the electronic structure remains the same, this should decrease S and induce a larger peak temperature, as explained above. However, our calculations show the opposite results for which, as we shall see, the TD distortion at the chemical potential can be account for.

Now, the increased bond length between atoms reduces hybridization, which gives rise to a narrower band dispersion as in Fig. 5(b) and high effective masses, and thus induces the smaller TD values as in Fig. 4(d). The effect in the electronic structure by the enlarged volume overcompensates the effect of a larger number of carriers/unit cell and results in a shallower chemical potential (a lower peak temperature) and a larger S. From Fig. 4(c), in the comparison of S for Bi_2Te_3 and Sb_2Te_3 with the same volume of V_{BT}, we see that Sb_2Te_3 exhibits a similar or even slightly higher S than that of Bi_2Te_3, which indicates that the volume effect is an important factor rather than different band structures to determine S in this same carrier concentration.

In the V_{avr} case of Bi_2Te_3, the volume reduction results in a lowering of S by 13 μV/K at 300 K and the shift of peak temperature from 400 to 425 K [Fig. 4(a)], which can be understood in the same way as with the above Sb_2Te_3 case. However, in Bi_2Te_3 case, the volume reduction by a smaller V_{ST} shows different results. In this case, the volume reduction shows S to be similar to the V_{BT} case at 300 K [Fig. 4(a)]. Compared to other volume changed cases, the relaxation effect of atomic positions in this case is largest and distinct from other cases.[28] Different from the band narrowing in the volume-dependent Sb_2Te_3 cases, this large relaxation shifts the highest valence band slightly up [compared to the previous VBM (along U-Γ) in the V_{BT} case] especially, along Γ-Z, Z-F, and Γ-L symmetry lines, in addition to the broader band dispersion [Fig. 5(a)]. Hence, in the case of the smaller volume effect in Bi_2Te_3, due to its large atomic relaxation effect, band structures should be carefully investigated instead of simply applying band broadening analysis, compared to the larger volume effect.[29]

Therefore, the volume effect can be an important part of an origin of the results that Bi doped into bulk Sb_2Te_3 or a deposition of thick layers of Bi_2Te_3 alternating with thinner layers of Sb_2Te_3, i.e., superlattices of Bi_2Te_3/Sb_2Te_3 can improve S, although they reduce σ. On the contrary, Sb doped into bulk Bi_2Te_3 or thick Sb_2Te_3 layers would contribute to a lower S but a higher σ. In addition, to improve S of bulk Sb_2Te_3, we can consider the inclusion of nanodots with a larger band gap, which does not affect the VBM of Sb_2Te_3 and a larger lattice constant compared to those of bulk Sb_2Te_3.

Thus, for enhancing the power factor (PF), an optimized Sb doping ratio in bulk Bi_2Te_3 or the thickness of Bi_2Te_3 layers in superlattices should be carefully controlled. To see this, the volume dependent PFs at 300 K were calculated at the different carrier concentrations of 10^{18}, 1.32×10^{19}, and 10^{20} cm^{-3}, where we used the constant relaxation time of 10^{-14} s for the calculation of σ in all cases. In bulk Bi_2Te_3, from Fig. 4(e), the smaller volume shows better PF especially at high carrier concentrations ($>10^{19}$ cm^{-3}). In this case, the effect of the volume change on the PF at the low carrier concentration of 10^{18} cm^{-3} is mainly manifested by S rather than σ. However, the PF at high carrier concentrations is improved mainly by σ through the volume reduction. In bulk Sb_2Te_3, from Fig. 4(f), the volume effect on the PF is much smaller compared to the Bi_2Te_3 case and the larger volume shows better PF at the high carrier concentration of 10^{20} cm^{-3}. Contrary to the above bulk Bi_2Te_3, the effect of the volume change on the PF at the low carrier concentrations of 10^{18} and 1.32×10^{19} cm^{-3} is mainly shown by σ but, at the high carrier concentration of 10^{20} cm^{-3}, it is mainly shown by S. Considering the decrease in the relaxation time at the larger carrier concentration, both the Bi_2Te_3 and Sb_2Te_3 appear to show the optimal carrier concentration of approximately 10^{19} cm^{-3}.

In summary, using a first-principles density-functional approach, we have calculated the transport coefficients for pure and mixed Bi and Sb tellurides. We showed that the carrier concentration, electronic structure, and volume have an important influence on the temperature dependent S, such as the peak location and the slope. We found that the optimal carrier concentration for the best power factor of Bi_2Te_3 and Sb_2Te_3 is approximately 10^{19} cm^{-3}. This may give a good insight to fabricate more efficient thermoelectric materials and devices.

*jhsong@pluto.phys.northwestern.edu

[1] D.-Y. Chung, T. Hogan, P. Brazis, M. Rocci-Lane, C. Kannewurf, M. Bastea, C. Uher, and M. G. Kanatzidis, Science **287**, 1024 (2000).

[2] T. M. Tritt and M. A. Subramanian, MRS Bull. **31**, 188 (2006).

[3] G. D. Mahan and J. O. Sofo, Proc. Natl. Acad. Sci. U.S.A. **93**, 7436 (1996).

[4] T. J. Scheidemantel, C. Ambrosch-Draxl, T. Thonhauser, J. V. Badding, and J. O. Sofo, Phys. Rev. B **68**, 125210 (2003).

[5] G. J. Snyder and E. S. Toberer, Nature Mater. **7**, 105 (2008).

[6] H. W. Jeon, H. P. Ha, D. B. Hyun, and J. D. Shim, J. Phys. Chem. Solids **52**, 579 (1991).

[7] A. Giani, A. Boulouz, B. Aboulfarah, F. Pascal-Delannoy, A. Foucaran, A. Boyer, and A. Mzerd, J. Cryst. Growth **204**, 91 (1999).

[8] J. Jiang, L. Chen, S. Bai, Q. Yao, and Q. Wang, J. Cryst. Growth **277**, 258 (2005).

[9] C. B. Satterthwaite and R. W. Ure, Jr., Phys. Rev. **108**, 1164 (1957).

[10] G. R. Miller and C. Li, J. Phys. Chem. Solids **26**, 173 (1965).

[11] H. Iwasaki, A. Ohishi, T. Kajihara, and S. Sano, Jpn. J. Appl. Phys., Part 1 **42**, 5477 (2003).

[12] R. Venkatasubramanian, E. Siivola, T. Colpitts, and B. O'Quinn, Nature (London) **413**, 597 (2001).

[13] P. Larson, S. D. Mahanti, and M. G. Kanatzidis, Phys. Rev. B **61**, 8162 (2000).

[14] S. Nakajima, J. Phys. Chem. Solids **24**, 479 (1963).

[15] T. L. Anderson and H. B. Krause, Acta Crystallogr., Sect. B: Struct. Crystallogr. Cryst. Chem. **30**, 1307 (1974).

[16] E. Wimmer, H. Krakauer, M. Weinert, and A. J. Freeman, Phys. Rev. B **24**, 864 (1981).

[17] H. J. F. Jansen and A. J. Freeman, Phys. Rev. B **30**, 561 (1984).

[18] M. Kim, A. J. Freeman, and C. B. Geller, Phys. Rev. B **72**, 035205 (2005).

[19] In Ref. 4, the calculated S and σ in the constant relaxation-time approximation show good agreement with experiment.

[20] The rigid-band model used in this work can be considered in the point (antisite) defect limit. Thus the electronic structure is not changed significantly in this limit. However, the rigid-band model is not expected to work well at high concentrations of defects/impurities due to the possible interactions between them. Indeed, the rigid-band model is known to work well up to the carrier concentration of 10^{20} cm^{-3} (Ref. 4).

[21] J. L. P. Hughes and J. E. Sipe, Phys. Rev. B **53**, 10751 (1996).

[22] The Bi and Sb tellurides show anisotropy in S and σ between basal plane and trigonal axis (c direction) (Ref. 4). We used the calculated S in the ab plane for comparison with experimental data since the directions of electrical current are parallel to the (111) cleavage planes. (Ref. 6, and references therein).

[23] B. M. Goltsman, B. A. Kudinov, and I. A. Smirnov, *Thermoelectric Semiconductor Material Based on* Bi_2Te_3 (Army Foreign Science and Technology Center, Charlottesville, VA, 1973).

[24] I. G. Austin, Proc. Phys. Soc. London **72**, 545 (1958).

[25] *Numerical Data and Functional Relationships in Science and Technology*, Landolt-Börnstein, New Series, Group III Vol. 17, Pt. F, edited by O. Madelung, M. Schulz, and H. Weiss (Springer, New York, 1983).

[26] S. J. Youn and A. J. Freeman, Phys. Rev. B **63**, 085112 (2001).

[27] P. Larson, Phys. Rev. B **74**, 205113 (2006).

[28] In the fixed structure, the calculated S is smaller than that of Bi_2Te_3 with a_{ave}/c_{ave} due to the volume effect.

[29] In Fig. 2(c), we can also see the similar behavior, where S of $(Bi_{0.5}Sb_{0.5})_2Te_3$ showing the large atomic relaxation is smaller than that of Sb_2Te_3 at the same carrier density, even though the volume of $(Bi_{0.5}Sb_{0.5})_2Te_3$ is larger than that of Sb_2Te_3.